Advanced Physical Research
Vol.5, No.2, 2023, pp.81-87

INFLUENCE OF CO-DOPING OF Y AND Fe ON STRUCTURAL AND FERROELECTRIC PROPERTIES OF $Ba_{1-x}Y_xTi_{1-x}Fe_xO_3$

T.A. Tran[1*], H.C. Tran[1], L.V. Truong-Son[2], D.T. Khan[2], N. Thanh-Nghiem[3], H.T. Phuc[4,5], D.P.T. Tien[6]

[1]Department of Physics, Ho Chi Minh City University of Technology and Education, Ho Chi Minh, Vietnam
[2]University of Science and Education, The University of Da Nang, Da Nang, Vietnam
[3]Graduate University of Science and Technology, Vietnam Academy of Science and Technology, Ha Noi, Vietnam
[4]Institute of Research and Development, Duy Tan University, Da Nang, Vietnam
[5]Laboratory Center, Duy Tan University, Da Nang, Vietnam
[6]Nhatrang Institute of Technology Research and Application, Vietnam Academy of Science and Technology, Nha Trang, Vietnam

Abstract. The structural and vibrational properties of polycrystalline samples $Ba_{1-x}Y_xTi_{1-x}Fe_xO_3$ ($0 \le x \le 0.2$) prepared using the solid-state reaction method have been investigated. X-ray diffraction (XRD) patterns revealed the presence of a persistent tetragonal phase (space group P4mm), which was significantly influenced by the concentration of Y and Fe dopants. Additionally, the ferroelectric polarization decreased as the dopant concentration increased. Raman studies indicated a change in the symmetry of the tetragonal phase as the dopant concentration increased, demonstrating a tendency to transform symmetrically into a cubic phase (space group *Pm-3m*). The surface morphology analysis exhibited an increase in the number of particles, compactness, and a decrease in particle size with increasing Y-Fe content.

Keywords: *$BaTiO_3$, ferroelectric, multiferroic materials, crystal structure, vibrational properties*

***Corresponding Author:** T.A. Tran, Department of Physics, Ho Chi Minh City University of Technology and Education, Ho Chi Minh 700000, Vietnam, e-mail: anhtt@hcmute.edu.vn*

***Received:** 18 January 2023; **Accepted:** 22 April 2023; **Published:** 23 June 2023.*

1. Introduction

Multiferroics coexist both magnetism and ferroelectricity, which have great potential for multistate memory elements, sensors, resonators, and tunable microwave devices such as filters and phase shifters (Khomskii, 2009; Dang *et al.*, 2011; Pyatakov & Zvezdin, 2012). Multiferroics ABO_3, in which A represents alkali or rare earth elements and B represents other transition metals, such as $BaTiO_3$, $SrTiO_3$, $PbTiO_3$ with perovskite structure have been widely used in nonlinear optics, thermoelectric detection, optoelectronic modulation, thin film capacitors, and optical memory. Their properties not only depend on crystal structure, shape, and size but also on the reduction of particle size to nanoscale (Dorfman *et al.*, 2001).

How to cite (APA): Tran, T.A., Tran, H.C., Truong-Son, L.V., Khan, D.T., Thanh-Nghiem, N., Phuc, H.T., & Tien, D.P.T. (2023). Influence of co-doping of Y and Fe on structural and ferroelectric properties of $Ba_{1-x}Y_xTi_{1-x}Fe_xO_3$. *Advanced Physical Research, 5*(2), 81-87.

Among the ABO_3 multiferroics, $BaTiO_3$ (BTO) has been extensively studied due to its remarkable dielectric, ferroelectric, and piezoelectric properties. BTO exhibits a low dielectric loss, a large electro-optic coefficient (Phan *et al.*, 2012), and a high dielectric constant. At room temperature, BTO undergoes a sequence of phase transitions: from rhombohedral to orthorhombic at -90°C, from orthorhombic to tetragonal at 5°C, from tetragonal to cubic at 130°C, from cubic to hexagonal at 1432°C, and from hexagonal to liquid at 1625°C (Chikada *et al*., 2010). These phase transitions are accompanied by changes in the magnetic and ferroelectric properties of the material.

Moreover, when doped with Mn, Fe, and Cr, BTO exhibits ferromagnetic behavior at room temperature (Mitra, 2012). Additionally, studies by Xu et al. have revealed the coexistence of ferroelectric and ferromagnetic properties in BTO doped with Fe (Xu *et al.*, 2009; Alshoaibi *et al.*, 2020). Doping Y into the Ba or Ti sites in BTO has been found to result in increased electrical conductivity, a large dielectric constant, and high dielectric loss. Furthermore, when BTO doped with Y is annealed above 1250°C, Y replaces the Ba site, transforming BTO into a semiconductor material (Qi *et al.*, 2003; Ren *et al.*, 2016).

Therefore, in this work, we investigate the effect of co-doping concentration on the crystal structure and ferroelectric properties of $Ba_{1-x}Y_xTi_{1-x}Fe_xO_3$ ($0 \leq x \leq 0.2$) materials using a combination of X-ray diffraction and Raman spectroscopy.

2. Experimental details

The polycrystalline samples of $Ba_{1-x}Y_xTi_{1-x}Fe_xO_3$ (BYTFO) (x = 0, 0.01, 0.02, 0.04, 0.06, 0.08, 0.1, 0.15, and 0.2) were synthesized by the solid-state reaction method, where the chemical ratio with a purity level of 99.99% comprising $BaCO_3$, TiO_2, Fe_2O_3, and Y_2O_3 (all from Sigma-Aldrich) was weighed and mixed for 10 hours using a planetary ball mill. After mixing and grinding, the mixture was pressed into pellets and pre-sintered at 1050°C for 24 hours. The sintered powders were reground and repellent for final sintering at 1300°C for 5 hours. The resulting sintered samples were then cooled to room temperature, and their surface morphology was observed using a scanning electron microscope (SEM). The phase composition and crystal structure were analyzed using a D8Advance Eco X-ray diffractometer (Bruker) equipped with a Cu-Kα radiation source (λ_1 = 1.5406 Å, λ_2 = 1.5444 Å with a ratio of intensity I_2/I_1 = 0.48). Rietveld refinement of the XRD data was performed using the FullProf software (Rodríguez-Carvajal, 1993). Raman spectra were obtained using a LabRAM Raman microscope with a He-Ne laser excitation wavelength of 532 nm.

3. Results and discussion

Fig. 1 depicts scanning electron microscopy (SEM) images of BYTFO samples for various values of x, including 0, 0.04, 0.08, and 0.1. From the images in Fig. 1, it is evident that the synthesized samples exhibit particles with irregular sizes and shapes. Notably, as the doping concentration x increases, there is a rapid decrease in particle size. In Fig. 1 (c) and (d), the presence of multiple stacked particles is observed, indicating that the surface morphology of BYTFO is strongly influenced by the concentrations of Y and Fe.

The crystal structure of the BYTFO materials was determined using the XRD method, and the results are presented in Fig. 2. The XRD patterns of the BYTFO samples

were analyzed using the Rietveld method, which demonstrates that all peaks correspond to a tetragonal structure with the symmetry of *P4mm* (according to JCPDS-792264), as illustrated in Fig. 3. It can be observed that all the samples exhibit a tetragonal perovskite structure without the presence of any secondary phases. This suggests that the doped ions have been fully incorporated into the unit cell, maintaining the perovskite structure of the solid solution.

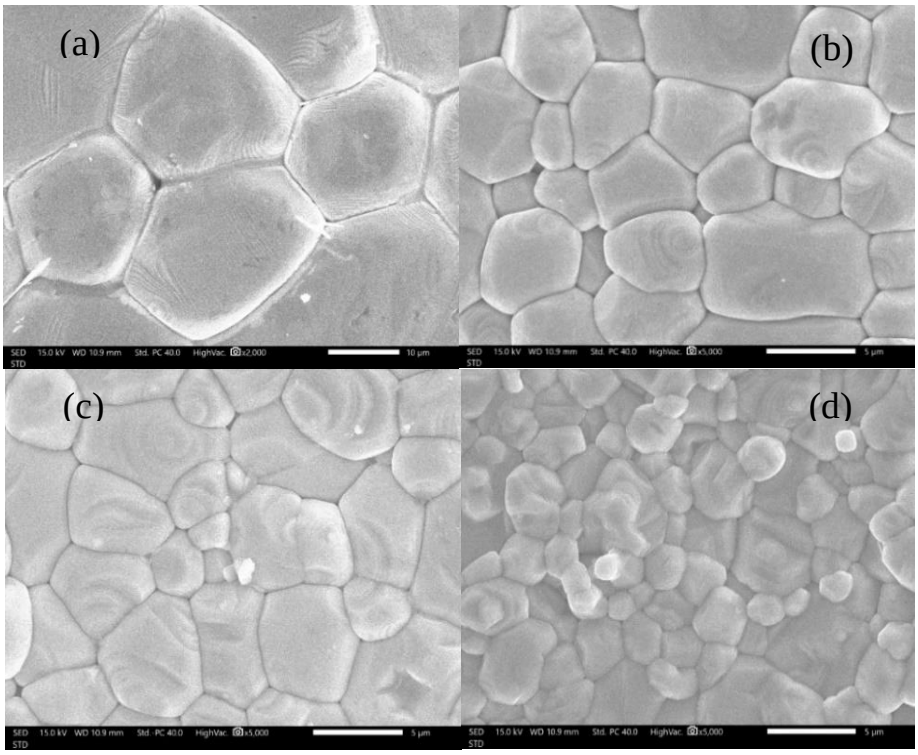

Fig. 1. Morphology of $Ba_{1-x}Y_xTi_{1-x}Fe_xO_3$ with corresponding values of *x*: (a) 0; (b) 0.04; (c) 0.08; (d) 0.1

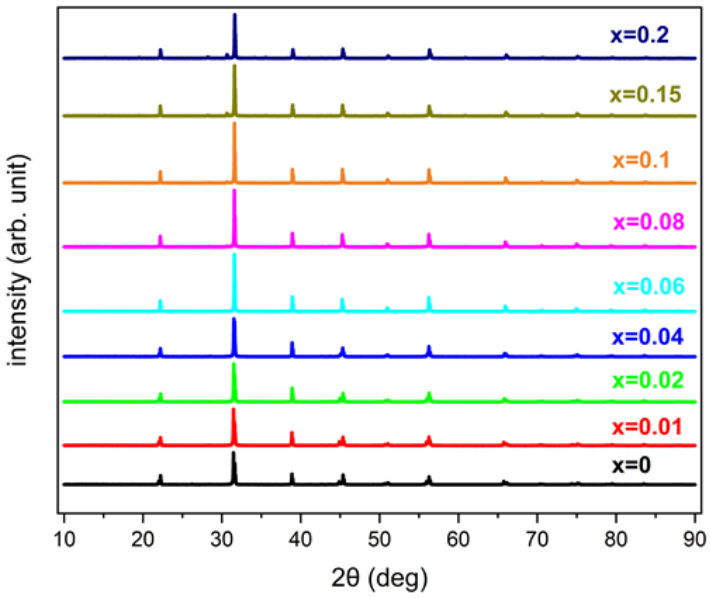

Fig. 2. X-ray diffraction patterns at room temperature of BYTFO samples. The experimental and calculated points are shown in the figure

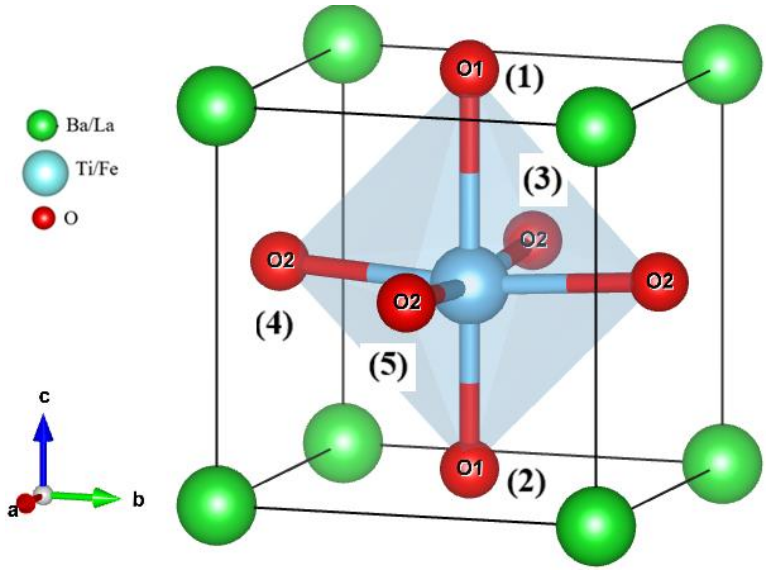

Fig. 3. Crystal structure of *P4mm* tetragonal phase

In the tetragonal structure of BYTFO, as depicted in Fig. 3, each barium ion is surrounded by 12 oxygen ions. Together, the oxygen and barium ions form a body-centered cubic lattice. The titanium ions occupy octahedral sites, which are surrounded by six oxygen ions. However, due to the comparatively larger size of the barium ions, the octahedral sites in BaTiO3 are relatively spacious for the titanium ions. As a result, the titanium ions tend to adopt energetically favorable off-center positions, displacing each of the surrounding six oxygen ions. This off-center displacement is facilitated by the titanium ions' charge of +4, leading to a significant degree of polarization. When an electric field is applied, the titanium ions are able to shift from their random positions to aligned positions, resulting in a substantial polarization effect and a high dielectric constant. This phenomenon is attributed to the movement of the titanium ions, driven by the applied electric field. Consequently, BaTiO3 exhibits a large polarization response. This behavior has been extensively studied and is associated with various applications (Khomskii, 2009; Dang *et al.*, 2011; Pyatakov & Zvezdin, 2012). The variation in bond length and angle of the sample can be observed in Table 1.

Table 1. Structural parameters, bond lengths, and bond angles of the BYTFO sample. Atom positions in *P4mm*: R (Ba/Y) 1a (0,0,0); M (Ti/Fe) 1b (0.5, 0.5, *z*); O1 1*a* (0.5, 0.5, *z*); and O2 2*c*(0.5, 0, *z*)

x	0	0.02	0.06	0.08	0.1	0.2
M1-O1(1) (Å)	2.0878(1)	2.0796(2)	2.0684(5)	2.0674(4)	2.0667(3)	2.0616(1)
M1-O1(2) (Å)	1.9476(1)	1.9399(2)	1.9294 (4)	1.9285(3)	1.9278(2)	1.9231(9)
M1-O2 (Å)	2.0072(1)	2.0084(1)	2.0088 (2)	2.0078(2)	2.0066(1)	2.0025(5)
O1(1)-M1-O2(5) (deg.)	84.138(4)	84.165(6)	84.195(7)	84.197(1)	84.196(7)	84.198(3)
O2(4)-M1-O2(5) (deg.)	89.402(5)	89.408(6)	89.414(2)	89.414(2)	89.414(9)	89.415(6)
O2(5)-M1-O1(2) (deg.)	95.862(4)	95.835(6)	95.802(1)	95.803(1)	95.804(7)	95.802(3)
R_p (%)	5.84	4.82	5.06	3.60	4.09	4.10
R_B (%)	8.15	7.87	8.64	6.19	6.86	6.77

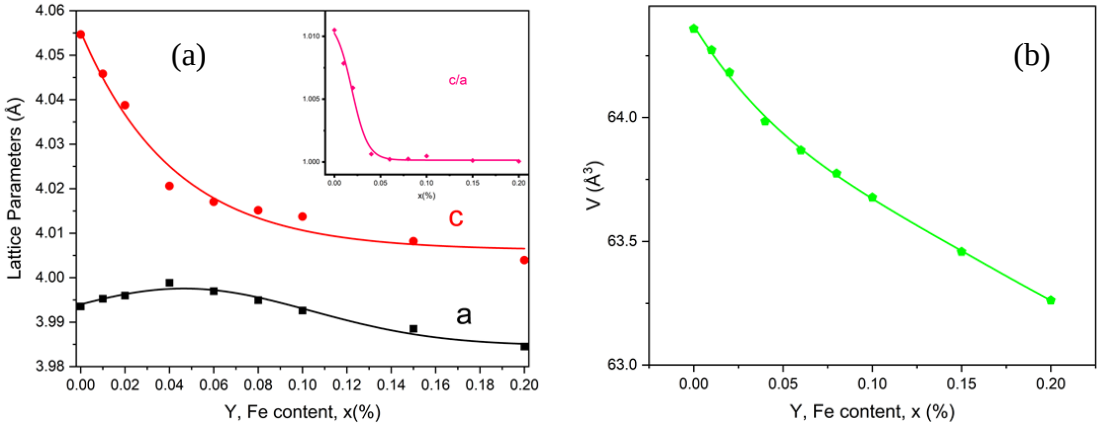

Fig. 5. The variation of unit-cell parameters (a) and volume (b) of BYTFO ceramic as a function of the Y and Fe doping concentration *x*. Inset of Fig. a: The evolution of the ratio *c*/*a* with respect to *x*

From XRD data refined using the Rietveld method, the dependence of the lattice parameters, unit cell volume, atomic positions, bond lengths, and bond angles on the doping concentration *x* are determined. The results are presented in Table 1, Figs. 5 and 6. As can be seen in Fig. 5, the lattice parameters *a*, *c*, *V*, and the deformation degree of unit-cell estimated through the ratio *c*/*a*, decrease with increasing the doping concentration *x*. This decrease of the lattice parameters is attributed to the smaller radii of Y and Fe compared with those of Ba and Ti. Similar to the lattice constants a and c, as the doping concentration increases the bond lengths of M - O1(1), M - O1(2) (along the *c* axis in Fig. 3) and M - O2 (in the *ab* plane in Fig. 3) decrease as shown in Fig. 6.

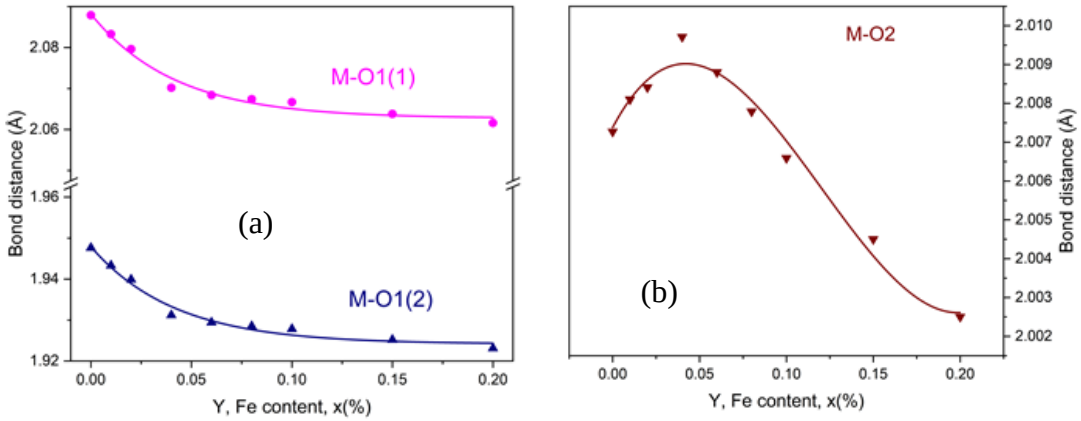

Fig. 6. Dependence on bond length M-O1(1), M-O2, M-O1(2)

Raman spectroscopy is a highly sensitive spectroscopic technique for probing the crystal structure of atoms in materials, so Raman studies have been conducted to gain a better understanding of the phase-related structure of Y and Fe co-doped $BaTiO_3$. The results are shown in Fig. 7. For the *P4mm* symmetry, first-order Raman-active modes are $\Gamma = 4E(TO+LO)+3A_1(TO+LO)+B_1(TO+LO)$ (Makovec, Samardžija and Drofenik, 2004; Park *et al.*, 2009). In Fig. 7, one can see that the Raman spectra of all synthesized sample are identical. These include a broad peak at around 264 cm^{-1}, a sharp peak at around 305 cm^{-1}, an asymmetric peak at around 514, and a broad peak at around 715 cm^{-1}that appears

together with other peaks, these peaks are characteristic of the tetragonal structure (symmetry P4mm) (Makovec *et al*., 2004; Park *et al.*, 2009). The broad peak at 264 cm^{-1} is assigned to the mode [$A_1(TO_2)$] correspondingly. The sharp peak at 305 cm^{-1} is assigned to the mode [E(TO) + E(LO) + B_1)]. An asymmetric maximum peak at 512 cm^{-1} is assigned to the mode [E(LO) + A_1(LO)] and a maximum peak at 717 cm^{-1} is assigned to the mode [E(LO)+A_1(LO)] (Narayanan & Vedam, 1961). The Raman spectra confirm that the BYTFO samples have a tetragonal structure consistent with the XRD results.

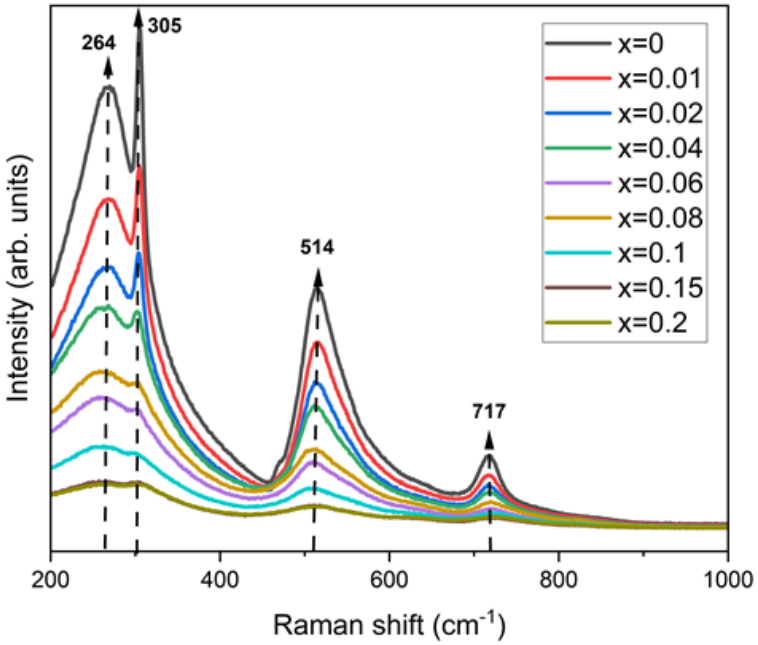

Fig. 7. Raman spectrum of the BYTFO

Although Raman spectra obtained from the BYTFO show no significant change in the notable wavelength shift, all Raman modes become weaker and broader with increasing dopant concentration. The broadening of Raman modes results from the appearance of structural disorder due to substitution with different valence or ion radii. These new/supplementary modes appear due to local phonon vibrations in the vicinity of the defect (substitution) or due to broken selection rules induced by defect-induced disorder (Pokorný *et al.*, 2011).

4. Conclusion

$Ba_{1-x}Y_xTi_{1-x}Fe_xO_3$ ceramics were synthesized by the solid-state phase method. X-ray diffraction (XRD) coupled with Raman spectroscopy analysis showed that all the samples had a tetragonal structure with *P*4*mm* symmetry. Scanning electron microscopy (SEM) revealed well-defined particles and a decrease in particle size as the amount of dopant concentration increases. In addition, the values of polarization decreased gradually as the amount of dopant concentration increases.

Acknowledgements

This work belongs to the project grant No: T2022-17 funded by Ho Chi Minh City University of Technology and Education (Vietnam).

References

Alshoaibi, A., Kanoun, M.B., Haq, B.U., AlFaify, S., & Goumri-Said, S. (2020). Insights into the impact of yttrium doping at the Ba and Ti sites of $BaTiO_3$ on the electronic structures and optical properties: A first-principles Study. *ACS Omega*, *5*(25), 15502-15509.

Chikada, S., Hirose, K., & Yamamoto, T. (2010). Analysis of local environment of Fe ions in hexagonal $BaTiO_3$. *Japanese Journal of Applied Physics*, *49*(9R), 091502.

Dang, N.V., Thanh, T.D., Hong, L.V., Lam, V.D., & Phan, T.-L. (2011). Structural, optical and magnetic properties of polycrystalline $BaTi_{1-x}Fe_xO_3$ ceramics. *Journal of Applied Physics*, *110*(4), 043914.

Dorfman, S., Fuks, D., Gordon, A., Kotomin, E., & Wyder, P. (2001). Some nonlinear properties of ferroelectric smart materials. *Physica B: Condensed Matter*, *304*(1-4), 339-347.

Khomskii, D. (2009). Classifying multiferroics: Mechanisms and effects. *Physics*, 2, 20.

Makovec, D., Samardžija, Z. & Drofenik, M. (2004). Solid solubility of holmium, yttrium, and dysprosium in $BaTiO_3$. *Journal of the American Ceramic Society*, *87*(7), 1324-1329.

Mitra, C. (2012). Nitrogen induced ferromagnetism in cobalt doped $BaTiO_3$. *AIP Advances*, *2*(3), 032148.

Narayanan, P.S., Vedam, K. (1961). Raman spectrum of strontium titanate. *Zeitschrift für Physik*, *163*(2), 158-164.

Park, K.-J., Kim, C.-H., Yoon, Y.-J., Song, S.-M., Kim, Y.-T., & Hur, K.-H. (2009). Doping behaviors of dysprosium, yttrium and holmium in $BaTiO_3$ ceramics. *Journal of the European Ceramic Society*, *29*(9), 1735-1741.

Phan, T.-L., Zhang, P., Grinting, D., Yu, S.C., Nghia, N.X., Dang, N.V., & Lam, V.D. (2012). Influences of annealing temperature on structural characterization and magnetic properties of Mn-doped $BaTiO_3$ ceramics. *Journal of Applied Physics*, *112*(1), 013909.

Pokorný, J., Pasha, U.M., Ben, L., Thakur, O.P., Sinclair, D.C., & Reaney, I.M. (2011). Use of Raman spectroscopy to determine the site occupancy of dopants in $BaTiO_3$. *Journal of Applied Physics*, *109*(11), 114110.

Pyatakov, A.P., Zvezdin, A.K. (2012). Magnetoelectric and multiferroic media. *Uspekhi Fizicheskih Nauk*, *182*(6), 593.

Qi, J., Li, L., Wang, Y., Fan, Y., & Gui, Z. (2003). Yttrium doping behavior in $BaTiO_3$ ceramics at different sintered temperature. *Materials Chemistry and Physics*, *82*(2), 423-427.

Ren, P., Wang, Q., Wang, X., Wang, L., Wang, J., Fan, H., Zhao, G. (2016). Effects of doping sites on electrical properties of yttrium doped $BaTiO_3$. *Materials Letters*, 174, 197-200.

Rodríguez-Carvajal, J. (1993). Recent advances in magnetic structure determination by neutron powder diffraction. *Physica B: Condensed Matter, 192*(1-2), 55-69.

Xu, B., Yin, K.B., Lin, J., Xia, Y.D., Wan, X.G., Yin, J., Bai, X.J., Du, J., Liu, Z.G. (2009). Room-temperature ferromagnetism and ferroelectricity in Fe-doped $BaTiO_3$. *Physical Review B*, *79*(13), 134109.